Frailty Subtypes and Recovery in Older Survivors of Acute Respiratory Failure. A Pilot Study.

Matthew R. Baldwin, MD, MS; Lauren R. Pollack, MD; Wendy C. Gonzalez, MD; Richard A. Friedman, PhD; Simone Norris, MS; Alka Javaid, BS; Max R. O'Donnell, MD, MPH; Matthew J. Cummings, MD; Dale Needham, MD, PhD; Elizabeth Colantuoni, PhD; Ursula M. Staudinger, PhD; Mathew S. Maurer, MD; David J. Lederer, MD, MS

SUPPLEMENTARY MATERIAL

TABLE OF CONTENTS

TABLE OF CONTENTS (CONTINUED)

E-METHODS

Enrollment of Participants

Exclusion criteria included: severe dementia based on a Clinical Dementia Rating score of >2.0; lives outside of the United States; undomiciled; does not speak English or Spanish; received lung transplantation; received extracorporeal membrane oxygenation for acute respiratory failure; required emergent cardiothoracic, abdominal, or vascular surgery; had pre-existing neurological injury or disease with motor deficits; respiratory failure due to a primary neurologic diagnosis; no surrogate; planned discharge to hospice at the time of enrollment.

Criteria for Querying the Surrogate

We asked the surrogate questions about the patient's baseline functional status for any patients who lacked capacity to sign informed consent, and in those who had cognitive impairment based on CAM-ICU or Mini-cog testing. If a surrogate was unsure about a patient's activities prior to hospitalization, we asked the surrogate to ask other family members or healthcare aides, or we asked permission from the surrogate to speak with other family members or healthcare aides who spent time with the patient prior to hospitalization. For prospective follow-up measurements of disability, we queried the surrogate who provided informed consent when the patient was not able to provide answers for him/herself.

Table E1. Assessment of Fried frailty phenotype criteria in older survivors of acute respiratory failure

Shrinking (weight loss)	Shrinking was defined as report as an unintentional weight loss of ≥ 10 pounds in the year prior to hospitalization involving intensive care. We asked the surrogate if the participant could not recall. We chose the year prior to hospitalization involving intensive care because weight changes during the index hospitalization may be confounded by treatments for critical illness (e.g. fluid resuscitation for shock, diuresis for pulmonary edema). In the rare instances when the participant and surrogate were unsure, we checked the electronic medical record outpatient notes for participants who received primary care through Columbia University Medical Center, and determined whether the participant lost 10 pounds or more in the year prior to hospitalization based on weights documented at outpatient visits.
Weakness (Decreased grip strength)	Weakness was assessed at the initial assessment during the week prior to hospital discharge while participants were on the general ward since making this measurement in the ICU is often not feasible because most patients are too critically ill to interact. We measured dominant hand grip dynamometry with the JAMAR Plus+ dynamometer (Patterson Medical, Illinois, USA), and calculated the average grip strength of 3 consecutive tests of maximum grip, as was done in the Cardiovascular Health Study (CHS). To assess the traditional frailty phenotype, weakness was defined based on the CHS criteria. Men met the criteria for weakness if their BMI and grip strength were ≤24 kg/m^2 and ≤29 kg; 24.1-26 kg/m^2 and ≤30 kg; 26.1-28 kg/m^2 and ≤31 kg; and >28 kg/m^2 and ≤32 kg, respectively. Women met the criteria for weakness if their BMI and grip strength were ≤23 kg/m^2 and ≤17 kg; 23.1-26 kg/m^2 and ≤17.3kg; 26.1-29 kg/m^2 and ≤18 kg; and >29 kg/m^2 and ≤21 kg, respectively (1).
Slowness (4.57-meter walk speed)	Slowness was assessed at the initial assessment during the week prior to hospital discharge while participants were on the general ward, since making this measurement in the ICU admission is often not feasible because most patients are too critically ill to walk. Participants were allowed up to 3 trials of walking 4.57 meters at a normal pace. We used the fastest walk time as the measurement of slowness. Participants were allowed to use canes or walkers, and those who required supplemental oxygen had their supply carried by a nurse assistant. Slowness was defined based on the CHS methodology. Men met criteria if height and walk time were ≤173 cm and ≥7 seconds, or >173 cm and ≥6 seconds, respectively. Women met criteria if height and walk time were ≤159 cm and ≥7 seconds, or >159 cm and ≥6 seconds,

	respectively.(1) Subjects who were unable to walk 4.57 meters with physical therapy had a gait speed of 0 m/s imputed and were considered slow.
Low Physical Activity	We chose to assess physical activity one month prior to hospitalization for both scientific and practical reasons. From a scientific perspective, in the Cardiovascular Health Study, Fried et al. intended to assess physical function in community-dwelling older adults at their baseline (1). Therefore, there is inherent validity in measuring older ICU survivors' function one month prior to hospitalization, since by doing so we capture these participants' baseline function. We substituted the Duke Activities Status Index for the Minnesota Leisure Time Physical Activity questionnaire, since in our prior work we showed that the DASI improves the construct and predictive validity of frailty assessments in ARF survivors (2). To assess the traditional frailty phenotype, low physical activity was defined based on our previously validated cutoffs (men, ≤12.5 units; women, ≤10 units) (2). We asked the surrogate about physical activity the month prior to hospitalization if the patient could not remember.
Exhaustion	Feelings of exhaustion were assessed at the initial assessment during the week prior to hospital discharge while participants were on the general ward. We chose to measure feelings of exhaustion during the post-ICU acute care period because we hypothesized feelings of fatigue after critical illness would hinder recovery. Furthermore, we felt that trying to remember and quantify subjective feelings prior to critical illness would predispose to recall bias. Exhaustion was defined as answers of 'moderate amount of time' or 'most of the time' to two statements from the modified 10-item Center for Epidemiologic Studies Depression Scale: "I felt everything I did was an effort for the past two days" and "I could not get going for the past two days" (3).

Additional Demographic and Clinical Variable Measurements

FOCIS-specific variables included the Acute Physiology and Chronic Health Evaluation (APACHE) II score, Charlson comorbidity index, type and duration of mechanical ventilation, and admission and discharge location.

Laboratory Measurements

Table E2. Commercial assays used for serum biomarker measurements

Biomarker	Type of Assay	Manufacturer	Manufacturer Location
IL-6	ELISA	R&D Systems	Minneapolis, MN, USA
TNFR1	ELISA	R&D Systems	Minneapolis, MN, USA
IGF-1	IDS-iSYS	Immunodiagnostics Systems	United Kingdom
DHEAs	chemiluminescent immunoassay	Siemens Healthcare Diagnostics	Deerfield, IL, USA
SHBG	chemiluminescent immunoassay	Siemens Healthcare Diagnostics	Deerfield, IL, USA
albumin	colormetic assay	Roche Diagnostics	Indianapolis, IN, USA

Quantitation of Testosterone using Liquid Chromatography-Mass Spectometry at the Columbia CTSA-Biomarker Core lab: The testosterone was extracted from human serum samples using liquid-liquid extraction. LCMS analysis were done using a triple quadrupole Waters Xevo TQ-S (Waters, Milford, MA) equipped with an electrospray ionization source and integrated with a Waters Acquity UPLC. Chromatographic separation was performed on a Waters C18 BEH column (2.1x100mm, 1.7µm, 130Å) with water and acetonitrile containing 0.1% formic acid as mobile phases. The mass spectrometer was operated under multiple reaction monitoring (MRM) mode with positive electrospray ionization and a MRM transition of 289.2>109.1.

Quantitation of 25-hydroxy vitamin D2 and D3 using Liquid Chromatography-Mass Spectometry at the Columbia University CTSA-Biomarker Core lab: 25-hydroxyvitamin D2 and 25-hydroxyvitamin D3 was measured using Ultra Performance Liquid Chromatography-Tandem Mass Spectrometry (LC-MSMS). 25OHD2 and 25OHD3

was extracted from human serum samples using liquid-liquid extraction and measured using a UPLC-MS/MS platform comprising a triple quadrupole Agilent 6410 mass spectrometer (Agilent, Santa Clara, CA) integrated to Agilent UPLC 1290 series. Chromatographic separation was performed by injecting 10uL of the extract onto a Agilent Poroshell 120 EC-C18 column (3.0 x 50mm, 2.7 µm) with water and methanol containing 0.1% formic acid as mobile solvents. The mass spectrometer was operated under multiple reaction monitoring (MRM) mode with positive electrospray ionization. MRM transitions were m/z 413->395 for 25-OH-D2, 401->383 for 25-OH-D3 and 407->389 for d6-25-OH-D3. Calibrators are standardized against the NIST standards.

Rationale for including cognitive impairment as a latent class indicator variable

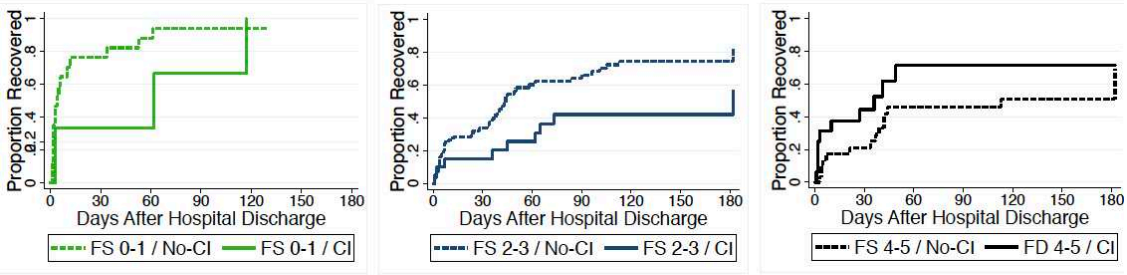

Figure E1. Kaplan Meier plots of recovery to pre-hospitalization Basic ADL function in FOCIS-I participants based on Fried Frailty Index scores using Cardiovascular Health Study criteria (grouped 0-1, 2-3, and 4-5), by the absence vs. presence of Cognitive Impairment (CI) at hospital discharge, p-for-interaction = 0.02. Cognitive impairment was defined as the presence of either delirium, assessed by the Confusion Assessment Method-ICU, or dementia, assessed by the Mini-Cog in those without delirium, during the baseline assessment that occurred on the medical ward during the week prior to hospital discharge.

Rationale for using serum exosomal proteomics

Serum exosomal proteomics is an innovative approach to investigate multisystem dysregulation from a peripheral blood sample (4, 5). Serum proteomics was previously limited because high abundance serum glycoproteins masked lower abundance proteins that may be

novel biomarkers (6-8). Exosomes are 30-100 nm vesicular bodies that are excreted from cells and can enter both neighboring cells and the systemic circulation (9). Exosomes have been recently recognized as a promising noninvasive diagnostic tool in critical illness (10), based on animal and human studies of acute lung injury and sepsis that indicate their involvement in relevant pathobiological functions of vital organs exposed to critical illness stressors (11-14). Protein ontology and pathway analysis of serum exosomal proteomic profiles of ARF survivors offers a systems biology approach to potentially elucidating further the multisystem dysregulation associated with frailty subtypes.

Selection of participants for serum exosome proteomics

Prior to the latent class identification of frailty subtypes, we selected 45 participants for serum exosome proteomics analysis. There were 20 who were not post-ICU frail and 25 who were post-ICU frail by the Fried phenotype criteria. We did not select anyone admitted from a skilled-care facility, and sought to match on age, sex, and pre-hospitalization ADL disability count (Table E4).

Exosome isolation

The Proteomics Shared Resource at Columbia University Medical Center isolated protein from exosomes, performed tandem mass spectroscopy (MS/MS), and identified and quantified exosome proteins.

Exosomes were isolated from 50 µl of participant serum using the Total Exosome Isolation Serum Kit (Invitrogen; ThermoFisher Scientific; Waltham, MA). Total exosome lysate was generated in 50 µl of lysis buffer (50mmlol/liter ammonium bicarbonate, 4 mol/liter urea, and a protease cocktail) using 1.4 mm ceramic beads and a rupture

homogenizer (OmniBead; Omni International, Eugene, OR). Protein concentration in total exosome lysate was determined using the Qubit Protein Assay Kit (Invitrogen; ThermoFisher Scientific; Waltham, MA).

Mass spectroscopy

Fifteen microliters of exosome lysate from each participant was digested by trypsin and labeled with the Amine-Reactive TMT10-plex Isobaric Mass Tag Labeling Regent Set (ThermoFisher Scientific; Waltham, MA) for MS/MS using the Thermo Orbitrap Fusion Tribrid Mass Spectrometer (ThermoFisher Scientific; Waltham, MA). The concentrated peptide mix was reconstituted in a solution of 2% acetonitrile and 2% formic acid for mass spectroscopy analysis. Peptides were loaded with the auto sampler directly on to a 2 cm C18 PepMap pre-column and were eluted from the15cm × 75μm inner diameter PepMap RSLC C18, 3 μm column with a 70-minute gradient from 2% Buffer B to 30% Buffer B (100% acetonitrile and 0.1% formic acid). The gradient was switched from 30% to 85% Buffer B over 5 minutes and held constant for 5 minutes. Finally, the gradient was changed from 85% Buffer B to 98% Buffer A (100% water and 0.1% formic acid) over 1 minute, and then held constant at 98% Buffer A for 8 more minutes. Application of a 2.0 kV distal voltage electrosprayed the eluting peptides directly into the Orbitrap mass spectrometer equipped with an Easy-Spray source (ThermoFinnigan, SanJose,CA). Full mass spectra were recorded on the peptides over a 400-to1,500 m/z range at 120,000 resolution, followed by MS/MS collision-induced dissociation (CID) events for a total cycle of 3 seconds. Charge state-dependent screening was turned off, and peptides with a charge state of 2 to 6 were analyzed.

Mass spectrometer scanning functions and high-performance liquid chromatography gradients were controlled by an Xcalibur data system (ThermoFinnigan, SanJose,CA). Three technical replicates were run for each sample.

Identification of proteins and their concentrations from MS/MS data.

MS/MS data from raw files were searched against FASTA-formatted sequences of the Uniprot human protein database (www.uniprot.org, January 29, 2017) using Proteome Discoverer software v2.2 (ThermoFisher Scientific; Waltham, MA). This application extracts relevant MS/MS spectra from the .raw file and determines the precursor charge state and the quality of the fragmentation spectrum. The software's probability-based score system rates the relevance of the best matches found by the SEQUEST algorithm (15). The peptide search tolerance was set to 10 ppm. A minimum sequence length of 7 amino acid residues was required. Only fully tryptic peptides were considered. To calculate of confidence levels and false discovery rates (FDR), Proteome Discoverer generates a decoy database containing reverse sequences of the non-decoy protein database and performs the search against this concatenated database (non-decoy + decoy) (16). The discriminant score was set at a 5% false discovery rate (FDR). Spectra counts were used as the quantitative values for the protein-based list.

Bioinformatics methods

Analyses were performed with packages in the R/Bioconcutor platform. Intensity values with technical replicates was imputed using the impute package. Qualities were assessed and outliers discarded using Principal Component Analysis (17),

Multidimensional Scaling (18), and Hierarchical clustering (19). All replicates were discarded for a patient containing a single replicate that was an outlier, unless doing so brought the number of patients in a frailty class below 3. After removing outliers, we had 112 samples from 36 patients.

We assessed individual proteome-wide differential protein expression between frailty subtypes using Limma (18), an empirical-Bayesian method (20, 21). The duplicate correlation method, an empirical Bayesian version of mixed-models, was used to include the effect of technical replication in the analysis (22). Given the low sample size and exploratory aim for these proteomic analyses, we set significance at $p < 0.05$ and a FDR < 0.2 and an absolute $\log_2$ fold change of > 0.2.

We conducted the unsupervised clustering analysis using the Cluster 3.0 package (23-25). We calculated the Euclidean distance (24) and performed k-means clustering (24, 26) with k=2 and k=100 iterations. We created heatmaps with protein expression centered using JavaTreeview (23, 27).

We also identified protein functional classes from the Reactome database that differed between frailty subtypes using the Correlation Adjusted Mean Rank gene set test (CAMERA) (28) at $p < 0.05$ and a FDR < 0.2. The pre-ranked mode of CAMERA based on the Limma results was used. We corrected for false discoveries by the method of Benjamini and Hochberg (29). The Reactome database is a peer-reviewed resource of human biological processes functions that can be used to discover functional relationships from expression profile data (30). We then identified those proteins differentially expressed according to Limma which belong to the Reactome protein

functional classes identified by CAMERA in order to identify which proteins may be operative in the differential protein functional classes.

Sensitivity analysis for time-aggregation Bias

The most commonly used time-to-event analyses (i.e. Cox proportional hazards model and Fine and Gray competing risk model) assume that the event of interest can occur along a continuum of time (i.e. time is continuous). However, this assumption that time is exactly or continuously measured is often not met in clinical studies with longitudinal follow-up for survey outcome measures. The limitation with having follow-up at fixed time points is that we cannot observe or realistically ask the participant to recall the exact day during the follow-up interval that she/he regained independence in a specific ADL. Therefore, we assume that the time to recovery is the time to the date of the assessment at which the participant reports having returned to an ADL disability count less than or equal to the pre-hospitalization count. This could result in bias in the effect estimates, called time-aggregation bias (31).

We sought to minimize time-aggregation bias with our fixed time point follow-ups of hospital discharge, and 1-month, 3-month, and 6-month post-hospital discharge follow-up by modeling time-to-recovery and time-to-death as time-in-days rather than discrete-time intervals. Specifically, we chose to model recovery after hospitalization as the time-in-days to the date of the follow-up assessment at which recovery was first achieved, and death after hospitalization as the time-in-days to the date of death, rather than assign a discrete-time interval for recovery or death based on the follow-up at which the event was ascertained (i.e. hospital discharge, 1-month, 3-month, or 6-month follow-up).

Modeling our recovery and death data as time-in-days to event, rather than a discrete-time to event intervals not only minimizes time-aggregation bias, but we believe that it is also the most transparent representation of the data. For example, the time intervals from ICU-discharge to hospital-discharge and hospital discharge to 1-month follow-up varied for participants (median (IQR): 7 (4-12) and 34 (31-42) days, respectively). Therefore, we felt that measuring this time-to-event for those who actually recovered to baseline by hospital discharge or 1 month was more accurately represented as the actual number of days, rather than a time-discrete interval (e.g. “1” for hospital discharge, “2” for 1-month follow-up). As another example, for those who died between the first and third month after hospital discharge, modeling time-to-death as the number of days to the date of death more accurately represents the time they survived rather than a time-discrete interval of “3” for assessing death at the 3-month follow-up visit.

Despite modeling recovery as time-in-days to event, we recognize that we are still assigning recovery times at the end of the appropriate interval of time. Therefore, our results may still be subject to time-aggregation bias. To assess the direction and magnitude of time-aggregation bias in our primary analysis, we conducted a sensitivity analysis that sought to minimize time-aggregation bias when using an estimator that assumes exact measurements of duration (31). For those who achieved recovery, we assigned the midpoint of the time interval between the date of the follow-up assessment at which recovery was ascertained and the date of the previous follow-up assessment at which recovery had not yet been achieved. An example calculation for a single patient who recovered is shown in the figure below.

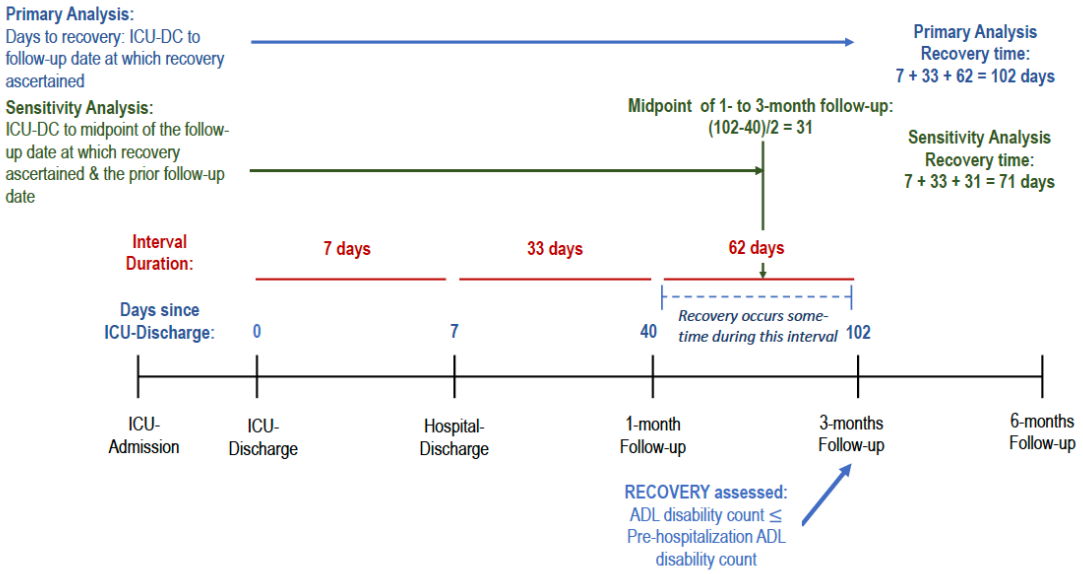

Figure. Example of how recovery time was calculated in the primary analysis versus sensitivity analysis that was done to assess for time aggregation bias due to interval follow-up.

SUPPLEMENT E-RESULTS

Table E3. List of latent class indicator variables included in latent class models.

Variable	Number of patients with data (total n = 185)	Number of patients with missing data	% missing data
Gait-speed	174	11	6.0%
Grip-Strength	180	5	0.54%
Duke Activity Status Index score	181	4	2.7%
Weight loss	182	3	1.6%
Cognitive impairment	176	9	4.9%

Table E4. Cytokine, vitamin D, and hormone levels during the week prior to hospital discharge in FOCIS study participants.

Hormone	IL-6 (pg/ml)	TNFR-1 (pg/ml)	25-hydroxy Vitamin D (ng/ml)	DHEAs (ug/ml)
All, median (IQR); mean (±SD)	12 (6.1-24); 23 (±46)	3193 (2375-5225); 5259 (±5667)	25 (18-32); 25 (±11)	
Men, median (IQR); mean (SD)				0.15 (0.15-0.37); 0.29 (±0.28)
Women, median (IQR); mean (±SD)				0.16 (0.15-0.27); 0.24 (±0.14)

Hormone	Total Testosterone (ng/ml)	Free-Testosterone (pg/ml)	IGF-1 (ng/ml)
All, median (IQR); mean (±SD)			
Men, median (IQR); mean (±SD)	1.68 (0.72-2.53); 1.82 (±1.38)	26.9 (13.3-45.1); 30.7 (±22.2)	61 (38-92); 69 (±43)
Women, median (IQR); mean (±SD)	0.081 (0.05-0.13); 0.12 (±0.17)	1.07 (0.50-1.86); 1.74 (±2.90)	60 (36-92); 69 (±44)

TNFR-1: Tumor necrosis factor soluble receptor 1. IL6: Interleukin-6.
DHEAs: dehydroepiandrosterone-sulfate. IGF-1: Insulin growth factor-1.
Free testosterone was calculated from total testosterone using the Vermeulen formula.

Table E5. Characteristics of n = 45 sub-sample of older acute respiratory failure survivors with serum exosome proteomics by frailty subtype

Characteristic	Subtype 1	Subtype 2	Subtype 3	Subtype 4	Subtype 5	p-value
Number of Subjects	16	9	11	5	4	
Demographics						
Age in years, mean (SD)	71 (10)	71 (6.4)	71 (4.5)	78 (7.8)	77 (5.5)	0.275
Male	7 (44)	3 (33)	5 (46)	2 (40)	2 (50)	0.977
Race						0.93
White	15 (94)	1 (11)	1 (9)	0 (0)	0 (0)	
Black	1 (6)	8 (89)	9 (82)	5 (100)	4 (100)	
Other	0 (0)	0 (0)	1 (9)	0 (0)	0 (0)	
Hispanic Ethnicity	9 (56)	5 (56)	10 (91)	1 (20)	3 (75)	0.073
Pre-hospital variables						
Residence						
Home	15 (100)	9 (100)	13 (100)	4 (100)	4 (100)	<0.001
Skilled-care facility	0 (0)	0 (0)	0 (0)	0 (0)	0 (0)	
ADL dependency count	0	0	0	1 (0-3)	0.5 (0-1)	0.046
Clinical Frailty Scale score	2 (2-2)	4 (-35)	3 (2-5)	5 (4-6)	6 (4-6)	0.001
Charlson Comorbidity Index Score	1 (0.5-2)	2 (1-3)	2 (1-4)	2 (1-5)	4.5 (3.5-5.5)	0.078
ICU variables						
APACHE II Score, mean (SD)	27 (6.3)	29 (11)	35 (8.8)	29 (4.3)	32 (5.4)	0.084
Type of Respiratory Support						0.6
Mechanical Ventilation	14 (88)	8 (89)	11 (100)	4 (80)	4 (100)	
Noninvasive Mechanical Ventilation Only	2 (12)	1 (11)	0 (0)	1 (20)	0 (0)	
ICU days	3 (2-6)	4 (3-6)	8 (7-16)	7 (3-8)	7 (3-13)	0.011
Post-ICU variables						
Post-ICU Frailty Phenotype score	1 (0-2)	3 (1-4)	3 (3-4)	4 (3-4)	3 (3-4)	0.0001
Cognitive Impairment*	2 (13)	1 (11)	5 (46)	0 (0)	4 (100)	0.002
ADL dependency count at hospital discharge	0 (0-2)	1 (0-2)	5 (2-6)	4 (3-5)	6 (6-6)	<0001
Total hospital days	9 (5-15)	11 (7-24)	20 (17-35)	18 (11-31)	17 (13-22)	0.027
Discharge Location						0.001
Home	15 (94)	7 (78)	4 (36)	1 (20)	1 (25)	
Skilled-care facility	1 (6)	2 (22)	7 (64)	4 (80)	3 (75)	
Died in 6 months	0 (0)	0 (0)	4 (36)	1 (20)	1 (33)	<0.001

Data are presented as n(%) or Median (IQR) unless otherwise stated. ADL: Activities of Daily Living. *Cognitive impaired defined as either delirium using the Confusion Assessment Method-ICU or dementia using the Mini-Cog test (score ≤2). Cognitive impairment assessments were conducted during the baseline assessment on the ward, after the ICU, during the week before hospital discharge.

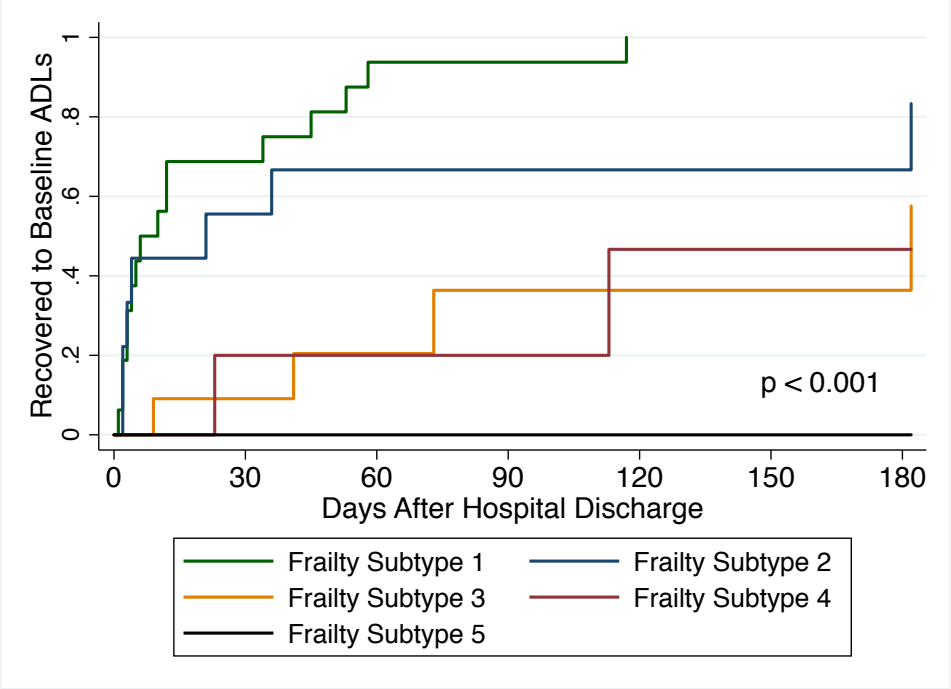

Figure E2. Kaplan-Meier cumulative incidence plots of frailty subtypes showing recovery to pre-hospitalization basic activities of daily living (ADLs) independence within 6-months after hospital discharge for the n = 45 sub-sample with serum exosome proteomics.

Table E6. Frailty subtype 1 serum exosomal differential protein expression and protein functional class regulation (compared to frailty subtype 2)

Exosomal proteome-wide differential protein expression identified with Limma (absolute log fold change >0.2 and FDR < 0.2)			
Count	Protein	Log Fold Change	FDR
1	KRT1	0.647	0.034
2	IGKV2D-24	-0.531	0.034
3	CP	0.257	0.034
4	KRT10	0.665	0.047
5	IGHV4-28	-0.398	0.074
6	A0A0G2JRQ6	-0.946	0.079
Differential Reactome protein functional classes regulation identified with CAMERA (FDR < 0.2)			
Count	Protein Functional Class	Direction of Regulation	FDR
1	**Immune System**		
2	REACTOME_INNATE_IMMUNE_SYSTEM	Down	0.034
5	REACTOME_COMPLEMENT_CASCADE	Down	0.034
3	REACTOME_REGULATION_OF_COMPLEMENT_CASCADE	Down	0.034
4	REACTOME_ACTIVATION_OF_NF_KAPPAB_IN_B_CELLS	Up	0.034
6	REACTOME_DOWNSTREAM_SIGNALING_EVENTS_OF_B_CELL_RECEPTOR_BCR	Up	0.034
7	REACTOME_SIGNALING_BY_THE_B_CELL_RECEPTOR_BCR	Up	0.034
8	REACTOME_CROSS_PRESENTATION_OF_SOLUBLE_EXOGENOUS_ANTIGENS_ENDOSOMES	Up	0.178
9	REACTOME_ANTIGEN_PROCESSING_CROSS_PRESENTATION	Up	0.094
10	REACTOME_ANTIGEN_PROCESSING_UBIQUITINATION_PROTEASOME_DEGRADATION	Up	0.065
11	REACTOME_VIF_MEDIATED_DEGRADATION_OF_APOBEC3G	Up	0.034
12	REACTOME_ER_PHAGOSOME_PATHWAY	Up	0.044
13	REACTOME_HIV_INFECTION	Up	0.063
14	REACTOME_HOST_INTERACTIONS_OF_HIV_FACTORS	Up	0.063
	Cell Cycle Functions		
15	REACTOME_CELL_CYCLE	Up	0.034
16	REACTOME_CELL_CYCLE_MITOTIC	Up	0.034
17	REACTOME_SIGNALING_BY_WNT	Up	0.034
18	REACTOME_CELL_CYCLE_CHECKPOINTS	Up	0.034
19	REACTOME_M_G1_TRANSITION	Up	0.034
20	REACTOME_G1_S_TRANSITION	Up	0.034
21	REACTOME_SYNTHESIS_OF_DNA	Up	0.034
22	REACTOME_MITOTIC_G1_G1_S_PHASES	Up	0.034
23	REACTOME_REGULATION_OF_MITOTIC_CELL_CYCLE	Up	0.034
24	REACTOME_MITOTIC_M_M_G1_PHASES	Up	0.034
25	REACTOME_ASSEMBLY_OF_THE_PRE_REPLICATIVE_COMPLEX	Up	0.034
26	REACTOME_DNA_REPLICATION	Up	0.034
27	REACTOME_MEIOSIS	Up	0.057
28	REACTOME_P53_DEPENDENT_G1_DNA_DAMAGE_RESPONSE	Up	0.034
29	REACTOME_P53_INDEPENDENT_G1_S_DNA_DAMAGE_CHECKPOINT	Up	0.034

30	REACTOME_CYCLIN_E_ASSOCIATED_EVENTS_DURING_G1_S_TRANSITION_	Up	0.034
31	REACTOME_AUTODEGRADATION_OF_THE_E3_UBIQUITIN_LIGASE_COP1	Up	0.034
32	REACTOME_S_PHASE	Up	0.034
33	REACTOME_MEIOTIC_RECOMBINATION	Up	0.081
34	REACTOME_CDK_MEDIATED_PHOSPHORYLATION_AND_REMOVAL_OF_CDC6	Up	0.034
35	REACTOME_CDT1_ASSOCIATION_WITH_THE_CDC6_ORC_ORIGIN_COMPLEX	Up	0.034
36	REACTOME_ORC1_REMOVAL_FROM_CHROMATIN	Up	0.034
37	REACTOME_APC_C_CDH1_MEDIATED_DEGRADATION_OF_CDC20_AND_OTHER_APC_C_CDH1_TARGETED_PROTEINS_IN_LATE_MITOSIS_EARLY_G1	Up	0.034
38	REACTOME_APC_C_CDC20_MEDIATED_DEGRADATION_OF_MITOTIC_PROTEINS	Up	0.034
39	REACTOME_AUTODEGRADATION_OF_CDH1_BY_CDH1_APC_C	Up	0.034
40	REACTOME_SCF_BETA_TRCP_MEDIATED_DEGRADATION_OF_EMI1	Up	0.034
41	REACTOME_SCFSKP2_MEDIATED_DEGRADATION_OF_P27_P21	Up	0.034
	Cellular Regulation and Gene Transcription		
42	REACTOME_REGULATION_OF_APOPTOSIS	Up	0.064
43	REACTOME_METABOLISM_OF_MRNA	Up	0.034
44	REACTOME_REGULATION_OF_MRNA_STABILITY_BY_PROTEINS_THAT_BIND_AU_RICH_ELEMENTS	Up	0.034
45	REACTOME_DESTABILIZATION_OF_MRNA_BY_AUF1_HNRNP_D0	Up	0.034
46	REACTOME_TRANSCRIPTION	Up	0.133
47	REACTOME_RNA_POL_I_RNA_POL_III_AND_MITOCHONDRIAL_TRANSCRIPTION	Up	0.133
48	REACTOME_RNA_POL_I_TRANSCRIPTION	Up	0.133
49	REACTOME_RNA_POL_I_PROMOTER_OPENING	Up	0.133
	Metabolism		
50	REACTOME_METABOLISM_OF_AMINO_ACIDS_AND_DERIVATIVES	Up	0.034
51	REACTOME_REGULATION_OF_ORNITHINE_DECARBOXYLASE_ODC	Up	0.068

Proteins differentially expressed by Limma that belong to Reactome functional protein classes identified by CAMERA

Protein	Protein Functional Class	Direction of Regulation	
KRT1	Innate immune system	Down	

Table E7. Frailty subtype 1 serum exosomal differential protein expression and protein functional class regulation (compared to frailty subtype 3)

Exosomal proteome-wide differential protein expression identified with Limma (absolute log fold change >0.2 and FDR < 0.2)			
Count	Protein	Log Fold Change	FDR
1	TGM4	-0.843	0.022
2	SERPINF2	-0.236	0.049
3	GSN	-0.386	0.056
4	SERPINA3	-0.382	0.056
5	FCGR3A	0.334	0.056
6	PIGR	0.585	0.056
7	CRISP3	-0.463	0.056
8	HRG	-0.318	0.056
9	KRT1	0.522	0.056
10	IGHV4-28	-0.373	0.057
11	SOWAHC	-1.497	0.077
12	FCGBP	0.541	0.077
13	IGFALS	-0.539	0.077
14	IGHV4-30-2	-0.462	0.099
15	SELENOP	-0.267	0.099
16	KRT10	0.536	0.100
17	CLEC3B	-0.309	0.131
18	KRT9	0.477	0.131
19	IGLV1-40	0.497	0.152
Differential Reactome protein functional classes identified with CAMERA (FDR < 0.2)			
Count	Protein Functional Class	Direction of Regulation	FDR
0			all >0.2
Proteins differentially expressed by Limma that belong to Reactome functional protein classes identified by CAMERA			
Protein	Protein Functional Class	Direction of Regulation	
None, because no differential protein functional classes were identified			

Table E8. Frailty subtype 1 serum exosomal differential protein expression and protein functional class regulation (compared to frailty subtype 4)

Exosomal proteome-wide differential protein expression identified with Limma (absolute log fold change >0.2 and FDR < 0.2)			
Count	Protein	Log Fold Change	FDR
1	IGKV4-1	-0.447	0.118
Differential Reactome protein functional classes identified with CAMERA (FDR < 0.2)			
Count	Protein Functional Class	Direction of Regulation	FDR
	Immune System		
1	REACTOME_INITIAL_TRIGGERING_OF_COMPLEMENT	Down	0.123
2	REACTOME_CREATION_OF_C4_AND_C2_ACTIVATORS	Down	0.154
Proteins differentially expressed by Limma that belong to Reactome functional protein classes identified by CAMERA			
Protein	Protein Functional Class	Direction of Regulation	
IGKV4-1	REACTOME_INITIAL_TRIGGERING_OF_COMPLEMENT	Down	
IGKV4-1	REACTOME_CREATION_OF_C4_AND_C2_ACTIVATORS	Down	

Table E9. Frailty subtype 1 serum exosomal differential protein expression and protein functional class regulation (compared to frailty subtype 5)

Exosomal proteome-wide differential protein expression identified with Limma (absolute log fold change >0.2 and FDR < 0.2)			
Count	Protein	Log Fold Change	FDR
1	FETUB	-1.136	0.033
2	TRAJ17	-1.419	0.033
3	MST1	0.588	0.033
4	LCN2	1.201	0.033
5	CRP	1.941	0.040
6	TTR	-0.769	0.065
7	SERPINF2	-0.318	0.065
8	IGLV1-40	0.903	0.065
9	SPRTN	2.210	0.068
10	IGLV2-18	0.993	0.106
11	NDST1	-0.547	0.120
12	C4B	0.611	0.120
13	TF	-0.554	0.120
14	KLKB1	-0.409	0.120
15	HPX	-0.563	0.120
16	IGLV3-10	-0.865	0.122
17	CLU	-0.297	0.122
18	ALB	-0.379	0.123
19	KNG1	-0.312	0.123
20	SELENOP	-0.383	0.134
21	SERPIND1	-0.702	0.138
22	PROC	-0.503	0.154
23	IGKV1D-33	0.752	0.161
24	AMBP	-0.365	0.161
25	AHSG	-0.503	0.177
26	SERPINA4	-0.436	0.177
27	GPX3	-0.562	0.200
28	ECM1	0.482	0.200
29	ORM2	-0.462	0.200
Differential Reactome protein functional classes identified with CAMERA (FDR < 0.2)			
Count	Protein Functional Class	Direction of Regulation	FDR
	Immune System		
1	REACTOME_COMPLEMENT_CASCADE	Down	0.173
2	REACTOME_ADAPTIVE_IMMUNE_SYSTEM	Up	0.173
3	REACTOME_ER_PHAGOSOME_PATHWAY	Up	0.173
4	REACTOME_ANTIGEN_PROCESSING_UBIQUITINATION_PROTEASOME_DEGRADATION	Up	0.173
5	REACTOME_DOWNSTREAM_SIGNALING_EVENTS_OF_B_CELL_RECEPTOR_BCR	Up	0.173
6	REACTOME_ACTIVATION_OF_NF_KAPPAB_IN_B_CELLS	Up	0.173
7	REACTOME_SIGNALING_BY_THE_B_CELL_RECEPTOR_BCR	Up	0.173
8	REACTOME_ANTIGEN_PROCESSING_CROSS_PRESENTATION	Up	0.173

9	REACTOME_CLASS_I_MHC_MEDIATED_ANTIGEN_PROCESSING_PRESENTATION	Up	0.173
10	REACTOME_CYTOKINE_SIGNALING_IN_IMMUNE_SYSTEM	Up	0.173
11	REACTOME_VIF_MEDIATED_DEGRADATION_OF_APOBEC3G	Up	0.173
12	REACTOME_HIV_INFECTION	Up	0.173
13	REACTOME_HOST_INTERACTIONS_OF_HIV_FACTORS	Up	0.173
	Cell Cycle Functions		
14	REACTOME_CELL_CYCLE_MITOTIC	Up	0.173
15	REACTOME_SIGNALING_BY_WNT	Up	0.173
16	REACTOME_ORC1_REMOVAL_FROM_CHROMATIN	Up	0.173
17	REACTOME_CELL_CYCLE	Up	0.173
18	REACTOME_P53_INDEPENDENT_G1_S_DNA_DAMAGE_CHECKPOINT	Up	0.173
19	REACTOME_CDK_MEDIATED_PHOSPHORYLATION_AND_REMOVAL_OF_CDC6	Up	0.173
20	REACTOME_CELL_CYCLE_CHECKPOINTS	Up	0.173
21	REACTOME_CYCLIN_E_ASSOCIATED_EVENTS_DURING_G1_S_TRANSITION_	Up	0.173
22	REACTOME_P53_DEPENDENT_G1_DNA_DAMAGE_RESPONSE	Up	0.173
23	REACTOME_M_G1_TRANSITION	Up	0.173
24	REACTOME_G1_S_TRANSITION	Up	0.173
25	REACTOME_CDT1_ASSOCIATION_WITH_THE_CDC6_ORC_ORIGIN_COMPLEX	Up	0.173
26	REACTOME_SYNTHESIS_OF_DNA	Up	0.173
27	REACTOME_AUTODEGRADATION_OF_THE_E3_UBIQUITIN_LIGASE_COP1	Up	0.173
28	REACTOME_MITOTIC_G1_G1_S_PHASES	Up	0.173
29	REACTOME_REGULATION_OF_MITOTIC_CELL_CYCLE	Up	0.173
30	REACTOME_MITOTIC_M_M_G1_PHASES	Up	0.173
31	REACTOME_ASSEMBLY_OF_THE_PRE_REPLICATIVE_COMPLEX	Up	0.173
32	REACTOME_APC_C_CDH1_MEDIATED_DEGRADATION_OF_CDC20_AND_OTHER_APC_C_CDH1_TARGETED_PROTEINS_IN_LATE_MITOSIS_EARLY_G1	Up	0.173
33	REACTOME_APC_C_CDC20_MEDIATED_DEGRADATION_OF_MITOTIC_PROTEINS	Up	0.173
34	REACTOME_AUTODEGRADATION_OF_CDH1_BY_CDH1_APC_C	Up	0.173
35	REACTOME_SCF_BETA_TRCP_MEDIATED_DEGRADATION_OF_EMI1	Up	0.173
36	REACTOME_S_PHASE	Up	0.173
37	REACTOME_SCFSKP2_MEDIATED_DEGRADATION_OF_P27_P21	Up	0.173
38	REACTOME_DNA_REPLICATION	Up	0.173
	Cellular Regulation and Gene Transcription		
39	REACTOME_METABOLISM_OF_MRNA	Up	0.173
40	REACTOME_METABOLISM_OF_RNA	Up	0.173
41	REACTOME_REGULATION_OF_MRNA_STABILITY_BY_PROTEINS_THAT_BIND_AU_RICH_ELEMENTS	Up	0.173
42	REACTOME_MEMBRANE_TRAFFICKING	Up	0.173

43	REACTOME_DESTABILIZATION_OF_MRNA_BY_AUF1_HNRNP_D0	Up	0.173
44	REACTOME_TRANS_GOLGI_NETWORK_VESICLE_BUDDING	Up	0.173
45	REACTOME_GOLGI_ASSOCIATED_VESICLE_BIOGENESIS	Up	0.173
	Metabolism		
46	REACTOME_REGULATION_OF_INSULIN_LIKE_GROWTH_FACTOR_IGF_ACTIVITY_BY_INSULIN_LIKE_GROWTH_FACTOR_BINDING_PROTEINS_IGFBPS	Down	0.173
47	REACTOME_REGULATION_OF_ORNITHINE_DECARBOXYLASE_ODC	Up	0.186
48	REACTOME_PTM_GAMMA_CARBOXYLATION_HYPUSINE_FORMATION_AND_ARYLSULFATASE_ACTIVATION	Down	0.173
49	REACTOME_GAMMA_CARBOXYLATION_TRANSPORT_AND_AMINO_TERMINAL_CLEAVAGE_OF_PROTEINS	Down	0.173

Proteins differentially expressed by Limma that belong to Reactome functional protein classes identified by CAMERA

Protein	Protein Functional Class	Direction of Regulation	
CLU	COMPLEMENT_CASCADE	Down	
CRP	COMPLEMENT_CASCADE	Down	
C4B	COMPLEMENT_CASCADE	Down	
LCN2	CYTOKINE_SIGNALING_IN_IMMUNE_SYSTEM	Up	
TF	MEMBRANE_TRAFFICKING	Up	

Table E10. Frailty subtype 2 serum exosomal differential protein expression and protein functional class regulation (compared to frailty subtype 3)

Exosomal proteome-wide differential protein expression identified with Limma (absolute log fold change >0.2 and FDR < 0.2)			
Count	Protein	Log Fold Change	FDR
1	PIGR	0.910817949	0.01931
2	FCGR2C	0.606356196	0.03191
3	CFHR4	-0.84133022	0.03191
4	HP	-1.230259491	0.05021
5	C9	-0.428717542	0.05993
Differential Reactome protein functional classes identified with CAMERA (FDR < 0.2)			
Count	Protein Functional Class	Direction of Regulation	FDR
0			all >0.2
Proteins differentially expressed by Limma that belong to Reactome functional protein classes identified by CAMERA			
Protein	Protein Functional Class	Direction of Regulation	
None, because no differential protein functional classes were identified			

Table E11. Frailty subtype 2 serum exosomal differential protein expression and protein functional class regulation (compared to frailty subtype 4)

Exosomal proteome-wide differential protein expression identified with Limma (absolute log fold change >0.2 and FDR < 0.2)			
Count	Protein	Log Fold Change	FDR
1	IGLV2-8	0.853430894	0.014
2	CP	-0.374654389	0.0195
3	VCL	0.720239874	0.0384
4	IGHV4-30-2	0.712998347	0.1187
Differential Reactome protein functional classes identified with CAMERA (FDR < 0.2)			
Count	Protein Functional Class	Direction of Regulation	FDR
0			all >0.2
Proteins differentially expressed by Limma that belong to Reactome functional protein classes identified by CAMERA			
Protein	Protein Functional Class	Direction of Regulation	
None, because no differential protein functional classes were identified			

Table E12. Frailty subtype 2 serum exosomal differential protein expression and protein functional class regulation (compared to frailty subtype 5)

Exosomal proteome-wide differential protein expression identified with Limma (absolute log fold change >0.2 and FDR < 0.2)			
Count	Protein	Log Fold Change	FDR
1	FETUB	-1.23286714	0.02667
2	LCN2	1.155408382	0.07211
3	AMBP	-0.469067214	0.1238
4	IGKV1D-33	0.864572367	0.14815
5	TGFBI	0.513221366	0.14815
6	IGLV2-18	1.153498669	0.14815
7	KLKB1	-0.44994892	0.14815
8	MST1	0.540726476	0.17023
9	IGKV1D-13	-2.267569247	0.17023
10	HPX	-0.700607707	0.17023
11	KNG1	-0.331515205	0.17023
12	IGHG4	1.485238115	0.17023
13	ITIH1	-0.415246292	0.17023
14	SERPINF2	-0.277060068	0.17023
15	PROZ	-1.102493098	0.17023
16	SERPIND1	-0.726648749	0.17023
17	SPRTN	1.754369604	0.20069
Differential Reactome protein functional classes identified with CAMERA (FDR < 0.2)			
Count	Protein Functional Class	Direction of Regulation	FDR
1	REACTOME_PTM_GAMMA_CARBOXYLATION_HYPUSINE_FORMATION_AND_ARYLSULFATASE_ACTIVATION	Down	0.0857
2	REACTOME_GAMMA_CARBOXYLATION_TRANSPORT_AND_AMINO_TERMINAL_CLEAVAGE_OF_PROTEINS	Down	0.0857
Proteins differentially expressed by Limma that belong to Reactome functional protein classes identified by CAMERA			
Protein	Protein Functional Class	Direction of Regulation	
PROZ	REACTOME_PTM_GAMMA_CARBOXYLATION_HYPUSINE_FORMATION_AND_ARYLSULFATASE_ACTIVATION	Down	
PROZ	REACTOME_GAMMA_CARBOXYLATION_TRANSPORT_AND_AMINO_TERMINAL_CLEAVAGE_OF_PROTEINS	Down	

Table E13. Frailty subtype 3 serum exosomal differential protein expression and protein functional class regulation (compared to frailty subtype 4)

Exosomal proteome-wide differential protein expression identified with Limma (absolute log fold change >0.2 and FDR < 0.2)			
Count	Protein	Log Fold Change	FDR
1	IGKV4-1	-0.4950067	0.02571
2	IGHV4-30-2	0.72774176	0.12816
3	SAA2-SAA4	1.06600823	0.12816
4	SAA1	1.83720225	0.12816
5	F13A1	-0.504736	0.14899
Differential Reactome protein functional classes identified with CAMERA (FDR < 0.2)			
Count	Protein Functional Class	Direction of Regulation	FDR
0			all >0.2
Proteins differentially expressed by Limma that belong to Reactome functional protein classes identified by CAMERA			
Protein	Protein Functional Class	Direction of Regulation	
None, because no differential protein functional classes were identified			

Table E14. Frailty subtype 3 serum exosomal differential protein expression and protein functional class regulation (compared to frailty subtype 5)

Exosomal proteome-wide differential protein expression identified with Limma (absolute log fold change >0.2 and FDR < 0.2)			
Count	Protein	Log Fold Change	FDR
1	IGLV3-10	-1.1356051	0.07302
2	FCGR3A	-0.5584034	0.07302
3	LCN2	1.10816193	0.07302
4	AHSG	-0.636413	0.12307
5	SPRTN	2.07023074	0.12307
Differential Reactome protein functional classes identified with CAMERA (FDR < 0.2)			
Count	Protein Functional Class	Direction of Regulation	FDR
0			all >0.2
Proteins differentially expressed by Limma that belong to Reactome functional protein classes identified by CAMERA			
Protein	Protein Functional Class	Direction of Regulation	
None, because no differential protein functional classes were identified			

There were no differentially expressed proteins nor Reactome protein functional classes comparing subtype 4 to subtype 5.

SUPPLEMENT REFERENCES

1. Fried LP, Tangen CM, Walston J, Newman AB, Hirsch C, Gottdiener J, Seeman T, Tracy R, Kop WJ, Burke G, McBurnie MA. Frailty in older adults: Evidence for a phenotype. *J Gerontol A Biol Sci Med Sci* 2001; 56A: M146-M156.

2. Baldwin MR, Singer JP, Huang D, Sell J, Gonzalez WC, Pollack LR, Maurer MS, D'Ovidio FF, Bacchetta M, Sonett JR, Arcasoy SM, Shah L, Robbins H, Hays SR, Kukreja J, Greenland JR, Shah RJ, Leard L, Morrell M, Gries C, Katz PP, Christie JD, Diamond JM, Lederer DJ. Refining Low Physical Activity Measurement Improves Frailty Assessment in Advanced Lung Disease and Survivors of Critical Illness. *Annals of the American Thoracic Society* 2017; 14: 1270-1279.

3. Orme JG, Reis J, Herz EJ. Factorial and discriminant validity of the Center for Epidemiological Studies Depression (CES-D) scale. *Journal of clinical psychology* 1986; 42: 28-33.

4. Raimondo F, Morosi L, Chinello C, Magni F, Pitto M. Advances in membranous vesicle and exosome proteomics improving biological understanding and biomarker discovery. *Proteomics* 2011; 11: 709-720.

5. Greening DW, Xu R, Gopal SK, Rai A, Simpson RJ. Proteomic insights into extracellular vesicle biology - defining exosomes and shed microvesicles. *Expert review of proteomics* 2017; 14: 69-95.

6. States DJ, Omenn GS, Blackwell TW, Fermin D, Eng J, Speicher DW, Hanash SM. Challenges in deriving high-confidence protein identifications from data gathered by a HUPO plasma proteome collaborative study. *Nature biotechnology* 2006; 24: 333-338.

7. Anderson NL, Anderson NG. The human plasma proteome: history, character, and diagnostic prospects. *Molecular & cellular proteomics : MCP* 2002; 1: 845-867.

8. Schiess R, Wollscheid B, Aebersold R. Targeted proteomic strategy for clinical biomarker discovery. *Molecular oncology* 2009; 3: 33-44.

9. Yanez-Mo M, Siljander PR, Andreu Z, Zavec AB, Borras FE, Buzas EI, Buzas K, Casal E, Cappello F, Carvalho J, Colas E, Cordeiro-da Silva A, Fais S, Falcon-Perez JM, Ghobrial IM, Giebel B, Gimona M, Graner M, Gursel I, Gursel M, Heegaard NH, Hendrix A, Kierulf P, Kokubun K, Kosanovic M, Kralj-Iglic V, Kramer-Albers EM, Laitinen S, Lasser C, Lener T, Ligeti E, Line A, Lipps G, Llorente A, Lotvall J, Mancek-Keber M, Marcilla A, Mittelbrunn M, Nazarenko I, Nolte-'t Hoen EN, Nyman TA, O'Driscoll L, Olivan M, Oliveira C, Pallinger E, Del Portillo HA, Reventos J, Rigau M, Rohde E, Sammar M, Sanchez-Madrid F, Santarem N, Schallmoser K, Ostenfeld MS, Stoorvogel W, Stukelj R, Van der Grein SG, Vasconcelos MH, Wauben MH, De Wever O. Biological properties of extracellular vesicles and their physiological functions. *Journal of extracellular vesicles* 2015; 4: 27066.

10. Terrasini N, Lionetti V. Exosomes in Critical Illness. *Crit Care Med* 2017; 45: 1054-1060.

11. Wu SC, Yang JC, Rau CS, Chen YC, Lu TH, Lin MW, Tzeng SL, Wu YC, Wu CJ, Hsieh CH. Profiling circulating microRNA expression in experimental sepsis using cecal ligation and puncture. *PloS one* 2013; 8: e77936.

12. Moon HG, Cao Y, Yang J, Lee JH, Choi HS, Jin Y. Lung epithelial cell-derived extracellular vesicles activate macrophage-mediated inflammatory responses via ROCK1 pathway. *Cell death & disease* 2015; 6: e2016.

13. Janiszewski M, Do Carmo AO, Pedro MA, Silva E, Knobel E, Laurindo FR. Platelet-derived exosomes of septic individuals possess proapoptotic NAD(P)H oxidase activity: A novel vascular redox pathway. *Critical care medicine* 2004; 32: 818-825.

14. Kovach MA, Singer BH, Newstead MW, Zeng X, Moore TA, White ES, Kunkel SL, Peters-Golden M, Standiford TJ. IL-36gamma is secreted in microparticles and exosomes by lung macrophages in response to bacteria and bacterial components. *Journal of leukocyte biology* 2016; 100: 413-421.

15. Yates JR, 3rd, Eng JK, McCormack AL, Schieltz D. Method to correlate tandem mass spectra of modified peptides to amino acid sequences in the protein database. *Analytical chemistry* 1995; 67: 1426-1436.

16. Elias JE, Gygi SP. Target-decoy search strategy for increased confidence in large-scale protein identifications by mass spectrometry. *Nature methods* 2007; 4: 207-214.

17. McDonald JW. affycoretools: Functions useful for those doing repetitive analyses with Affymetrix GeneChips. 1.52.2 ed; 2018.

18. Ritchie ME, Phipson B, Wu D, Hu Y, Law CW, Shi W, Smyth GK. limma powers differential expression analyses for RNA-sequencing and microarray studies. *Nucleic acids research* 2015; 43: e47.

19. R Core Team. R: A Language and Environment for Statistical Computing}. 3.5.2 ed. Vienna, Austria: R Foundation for Statistical Computing; 2018.

20. Smyth GK. Linear Models and Empirical Bayes Methods for Assessing Differential Expression in Microarray Experiments. *Statistical Applications in Genetics and Molecular Biology* 2004; 3: Article 3, http://www.bepress.com/sagmb/vol3/iss1/art3/.

21. Ritchie ME, Diyagama D, Neilson J, van Laar R, Dobrovic A, Holloway A, Smyth GK. Empirical array quality weights in the analysis of microarray data. *BMC bioinformatics* 2006; 7: 261.

22. Smyth GK, Michaud J, Scott HS. Use of within-array replicate spots for assessing differential expression in microarray experiments. *Bioinformatics* 2005; 21: 2067-2075.

23. Eisen MB, Spellman PT, Brown PO, Botstein D. Cluster analysis and display of genome-wide expression patterns. *Proc Natl Acad Sci USA* 1998; 95: 14863-14868.

24. Everitt BS, Landau S, Leese M. Cluster Analysis. Wiley; 2011.

25. de Hoon MJ, Imoto S, Nolan J, Miyano S. Open source clustering software. *Bioinformatics* 2004; 20: 1453-1454.

26. Lloyd SP. Least square quantization in PCM. *IEEE Transactions on Information Theory* 1957; 28: 129–137.

27. Saldanha AJ. Java Treeview--extensible visualization of microarray data. *Bioinformatics* 2004; 20: 3246-3248.

28. Wu D, Smyth GK. Camera: a competitive gene set test accounting for inter-gene correlation. *Nucleic acids research* 2012; 40: e133.

29. Benjamini Y, Hochberg Y. Controlling the false discovery rate; A practical and powerful approach to multiple testing. *J Roy Stat Soc Ser B* 1995; 57: 289-300.

30. Matthews L, Gopinath G, Gillespie M, Caudy M, Croft D, de Bono B, Garapati P, Hemish J, Hermjakob H, Jassal B, Kanapin A, Lewis S, Mahajan S, May B, Schmidt E, Vastrik I, Wu G, Birney E, Stein L, D'Eustachio P. Reactome knowledgebase of human biological pathways and processes. *Nucleic acids research* 2009; 37: D619-622.

31. Petersen T. Time-Aggregation Bias in Continuous-Time Hazard-Rate Models. *Sociological Methodology* 1991; 21: 263-290.